# Estimation of the Hottest Spot Temperature (HST) in Power Transformers Considering Thermal Inhomogeniety of the Windings

M. K. Pradhan and T. S. Ramu

***Abstract*—The degradation of electrical insulation in transformers is traced to thermoelectric processes. Existence of localized hot regions due to thermal insulating properties of electrical insulation would cause thermal runaway around these regions. In an earlier paper [1], the authors presented analytical methods for estimating the temperature and its distribution at different points of the transformer based on a closed-form mathematical technique using a generalized heat conduction (GHC) model. Certain aspects of the inhomogeniety of the several components of the winding and incorporation of distributed heat source were not addressed. Also, a rigorous treatment involving the changes in winding resistance, which was built into the thermal model as an empirical correction factor, has now been modified and incorporated in the GHC. These considerations have now improved the accuracy of estimation of hottest spot temperature.**

***Index Terms*—Location of hottest spot temperature (HST), prediction accuracy, transformer insulation, winding thermal conductivity.**

## NOMENCLATURE

| | |
|---|---|
| $a, b$ | Inner and outer radius of the annular disc or layer. |
| $n, m$ | Index to roots of transcendental (19) and (20). |
| $\tau$ | Time constant of the solid part of insulation. |
| $\ell$ | Thickness of the disc or height of layer winding. |
| $\alpha_d$ | Diffusivity of insulation-conductor system $\mathrm{m}^2/\mathrm{s}$. |
| $\check{\alpha}_d$ | $\frac{1}{\rho_{\mathrm{eq}} C p_{\mathrm{eq}}} = \frac{\alpha_d}{\mathbf{K}}$ (shown in Section II-D-I). |
| $\varrho_t$ | Coefficient for resistance change to temperature $^\circ\mathrm{C}^{-1}$. |
| $\psi(r)$ | Polynomial of $r$. |
| $\phi(z)$ | Polynomial of $z$. |
| $\beta_n$ | Roots of transcendental (19). |
| $\alpha_m$ | Roots of transcendental (20). |
| $\mathbf{M}(\alpha_m, z)$ | Kernel function for finite Fourier transform (FFT) |
| $\mathbf{K}_0(\beta_n, r)$ | Kernel function for finite Hankel transform (FHT). |
| $\mathbf{N}/\mathbf{N}'$ | Orthonormal incase of FHT/FFT. |
| $k_i, h_i, \mathbf{f}_i$ | Thermal conductivity, heat transfer coefficient, and boundary function at different surfaces of annular cylinder, $i = 1, 2 \rightarrow$ inner, outer cylindrical surfaces, $i = 3, 4 \rightarrow$ bottom, top surfaces |
| $\mathbf{K}_{\mathrm{ten}}$ | Thermal conductivity tensor. |
| $k_r, k_z$ | Principal thermal conductivity in radial and axial direction $k_r = k_1 = k_2$ and $k_z = k_3 = k_4$. |
| $\mathbf{K}$ | Referred to as equivalent thermal conductivity. |
| $\mathbf{f}_i^{(I)}$ | Temperature along the axial direction at $t = 0$. |
| $\mathbf{f}_i^{(F\sim I)}$ | Difference of temperature along axial direction at final state $t = \infty$ and initial state $t = 0$. |
| $r_i$'s | $i = 1, 2 \ldots$, radii of insulation and conductor layers. |
| $m_{si}$ | Oil temperature gradient along axial direction $^\circ\mathrm{C}/\mathrm{m}$. |
| $t_{\mathrm{cu}}/t_{\mathrm{kp}}$ | Thickness of conductor, kraft paper, $t_{pb} \rightarrow$ press board. |
| $\overline{\overline{\mathbf{G}}}_0$ | Combine Fourier and Hankel transform of heat source function $\mathbf{G}_0$. |
| $\mathbf{g}_0$ | Heat source $G$ at temperature $T = T_0$. |
| $\overline{\overline{\mathbf{F}}}$ | Combine Fourier and Hankel transform of initial function $\mathbf{F}(r, z)$. |
| $T_{\mathrm{b}}, T_{\mathrm{top}}$ | Temperature at the bottom and top of the winding. |
| $q_w$ | Heat flux in $\mathrm{wm}^{-2}$. |
| $V_{\mathrm{oil}}$ | Oil velocity inside the cooling duct, m/s. |
| $k_{\mathrm{kp}}, k_{\mathrm{pb}}$ | Thermal conductivity of kraft paper and pressboard. |
| $k_{\mathrm{cu}}$ | Thermal conductivity of copper $\mathrm{W}/\mathrm{m}^\circ\mathrm{C}$. |
| hvD | High-voltage disc winding. |
| lv2L | Second layer of low-voltage winding. |
| $\mathrm{loc}(\mathcal{R}/\mathcal{L})$ | Radial/ axial location of hot spot (in Tables III–V. |
| OD | Directed oil-forced cooling. |
| ND | Nondirected oil-forced cooling. |
| ONAN | Oil natural and air natural cooling. |
| ONAF | Oil natural and air-forced cooling. |

Manuscript received February 3, 2003; revised May 23, 2003. Paper no. TPWRD-00039-2003.

The authors are with the Department of High Voltage Engineering. Indian Institute of Science, Bangalore 560012, India (e-mail: manoj@hve.iisc.ernet.in).

Digital Object Identifier 10.1109/TPWRD.2004.835291

## I. INTRODUCTION

TRANSFORMERS are important and expensive elements of a power system. Inordinate localized temperature rise (HST) causes rapid thermal degradation of insulation and subsequent thermal breakdown. In order to draw maximum power from station transformers and, at the same time, avoid thermal mishaps, it is essential to carefully study its thermal behavior in all its entity.

To prescribe the limits of short-term and long-term loading capability of a transformer, it is necessary to estimate the hottest spot temperature (HST) of transformer winding to as high a degree of accuracy as can possibly be made. Furthermore, an accurate computation of the HST helps in a realistic estimation of

the reliability and remaining life of the transformer winding insulation.

A perusal of current literature in this area indicates that in the recent past, conventional heat run tests performed after the transformer was manufactured were the only means of acquiring information on the magnitude of the possible HST, but the location of HST was not possible. The extrapolation of heat run test results to quantify the amount of insulation degradation was found to be highly inaccurate [2]–[5].

Recently, various methods have been suggested for direct measurements of HST in transformer windings using fiber-optic sensors and fluoro-optic thermometers and the optimal location of these sensors has also been demonstrated. It has been reported [6], [7] that optoelectronic modules have since been introduced in the full-size transformers.

Certain empirical formulae have been proposed [4], [8], [11] whereby transformer designers could estimate possible maximum winding temperature at the design stage. These formulae, although not very accurate, serve as broad guidelines for verifying the designs.

It is therefore important to note that a worthwhile treatment of the thermal aspects of a transformer has been made only very recently [9], [10] wherein a semitheoretical model has been proposed to study certain aspects of heat transfer in cylindrical geometries. A comprehensive report generated by the CIGRE working group 12, examines, critically, all aspects of diagnosis of power transformers to show that the conventional factory heat run test and/or gas analysis fail to provide information on the magnitude of HST and overloading limits [2], [3]. In continuation to the IEEE Transformer loading guide [8], a recent addendum [12] to it gives further information on thermal modeling of a power transformer. An equivalent circuit analogy of transformer model considered by Swift *et al.* [13].

Admittedly, these models are mathematically much simpler. The calculation of average bulk oil and winding temperature can be made, knowing the thermal capacity of the solid (winding) or liquid (oil) medium. Since the masses of winding and oil bulk are known from the design, the heat capacity of bulk oil and winding can be easily calculated. These models present difficulties when used to estimate temperature of the hottest spot, or top-oil temperature.

Earlier work in this area [1], [14] assumes a constant heat source operating over the entire winding structure, besides treating the winding to be thermally isotropic. Also, a single empirical heat-transfer formula suggested thus far for calculating the boundary layer temperature drop has been applied to all surfaces of the winding [14]. But this is found to be incorrect as the mechanism of natural heat convection in the axial direction is markedly different from that along the radial direction. Such an assumption holds true for layer-type winding only.

In a recent paper [1], the authors proposed a procedure for predicting HST in the winding based on a generalized boundary value problem (BVP) of heat conduction with certain simplifying assumptions as detailed therein. It was observed that a far greater accuracy of estimation of HST as well as top oil temperature (TOT) is possible if certain changes are incorporated in the thermal model. The authors have now embarked on a technique for improving the accuracy of predicting the magnitude and the location of the HST. This calls for a major revision of the thermal model considering the following changes.

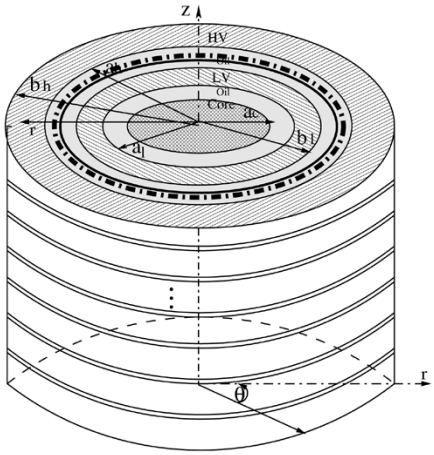


Fig. 1. Simple model of transformer winding, HV = disc, LV = layer.

- The transformer winding shall be treated as a thermally anisotropic structure which is actually true in practice.
- The heat source shall be considered as a function of the local temperature (distributed heat source).
- As opposed to the earlier treatment, the initial temperature distribution function should be rewritten as a new function of the curvature of the transformer winding as shown later.

It has been demonstrated that with these modifications, the magnitude, as well as the location of HST and the spatial temperature distribution in transformer windings could be estimated much more accurately than could be done until now.

In their earlier work, the thermal time constant $(\tau)$ of the winding was assumed to be a notional value of 5 min. In this paper, it has been expressly shown that $\tau$ has indeed a value in the neighborhood of 5 min in most cases.

## II. Formulation of the BVP of HCE of a Transformer Winding Taking Thermal Anisotropy Into Account

### A. Simplified Transformer Winding

The structure of a transformer winding is complex and does not conform to any known geometry in the strict sense. Under fairly general conditions, the transformer windings can be assumed cylindrical in formation; hence, a layer or a disc winding is considered to be a finite annular cylinder. The thermal and physical properties of the system would be equivalent to a composite system of insulation and conductor. A simple geometry of a model transformer winding is given in Fig. 1.

In the current paper, the heat generated in the body of the winding is taken to be a function of the local temperature [see (9)]. The heat is conducted away from here by the insulating oil in constant circulation in the vertical and horizontal ducts by a process of convection. However, in an actual transformer, the copper conductor is the heat source and is distributed over the volume of the cylinder defining the winding geometry. The heat generated in insulation due to dielectric loss is normally ignored.

The process of heat transfer in transformers is due both to conduction and to convection. The mixed boundary value

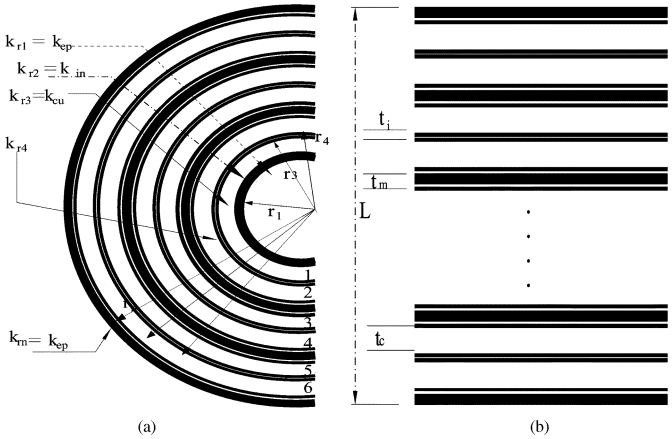


Fig. 2. (a) Horizontal cross-sectional view of a disc winding with six radial layer. (b) Vertical cross-section of a layer winding.

problem describing the process herein, automatically takes care of both the modes of heat transfer. The convection formulae for the calculation of heat-transfer coefficients have been given in the authors' earlier paper [1]. To avoid repetition, these formulae are not included here.

As opposed to the earlier formulations [1], the thermal conductivity in the radial and axial directions have been taken, more rigorously, to be functions of the spatial coordinates of that point and, hence, implying anisotropy. However, in view of axial symmetry of the winding, the temperature is treated as being independent of space variable $\theta$. The temperature at any point on the periphery of circle for a specific value of $r$ and $z$ is deemed a constant (i.e., presence of spacers have been ignored). With this assumption, the BVP can be reduced to a two-dimensional (2-D) problem.

**Improved Method of Calculation of Equivalent Thermal Conductivity**

Thermal conductivity (**t.c.**) of a disc or a layer in the radial direction has been calculated using the logarithmic formula (1). The thickness of the copper-insulation layers, as shown in Fig. 2(a), can be calculated from the design data of the winding

$$k_r = \frac{\log \frac{r_n}{r_1}}{\left( \frac{\log \frac{r_2}{r_1}}{k_{r1}} + \frac{\log \frac{r_3}{r_2}}{k_{r2}} + \cdots + \frac{\log \frac{r_n}{r_{n-1}}}{k_{rn}} \right)}. \tag{1}$$

Similarly, the **t.c.** of a disc or layer in $z$-direction can be calculated as in (2) [Fig. 2(b)]

$$k_z = \frac{k_{cu}k_{kp}k_{pb}(t_{cu} + t_{kp} + t_{pb})}{t_{kp}k_{cu}k_{pb} + t_{cu}k_{kp}k_{pb} + t_{pb}k_{kp}k_{cu}}; \tag{2}$$

where $t_{\rm cu}$, $t_{\rm kp}$, and $t_{\rm pb}$ are total thickness of copper, kraft paper, and pressboard in axial direction, respectively. The calculated effective thermal conductivity of a typical power transformer windings in axial and radial direction has been given in Table I. These values have been used in the computation of HST.

TABLE I
TYPICAL VALUES OF $k_z$ AND $k_r$ OF TRANSFORMER WINDINGS

| $k_r$ $W/m^0C$ | $k_z$ $W/m^0C$ | $\mathbf{K}$ $W/m^0C$ | winding type | transformer rating(MVA) | Manuf-acturer |
|---|---|---|---|---|---|
| 2.8 | 1.4 | 1.98 | Hv disc | 22.5 | I |
| 4.5 | 1.58 | 2.67 | Lv disc | 22.5 | I |
| 2.5 | 4.4 | 3.32 | Hv disc | 25/32 | II |
| 7.2 | 4.46 | 5.67 | Lv layer | 25/32 | II |
| 7.35 | 4.46 | 5.72 | Lv layer | 25/32 | II |

### *B. Methods of Treating the Anisotropy in Thermal Conductivity*

In fact, the vastly varying thermal conductivity can be incorporated in BVP directly. This can be easily taken care of by recognizing the fact that the winding is a thermally inhomogeneous structure and, hence, the thermal conductivity should be treated as a tensor. Accordingly, the governing equations are to be rewritten to account for the anisotropy. With this change, the thermal conductivity takes the following form:

$$\mathbf{k}_{\rm ten} = \begin{vmatrix} k_{rr} & k_{rz} \\ k_{zr} & k_{zz} \end{vmatrix}$$

where $k_{rr} \ldots k_{zz}$ are called conductivity coefficients. Considering the transformer winding (simplified as above), the insulation structure closely satisfies the orthotropic structure in the orthogonal coordinate system and the above equation becomes

$$\mathbf{k}_{\rm ten} = \begin{vmatrix} k_{rr} & 0 \\ 0 & k_{zz} \end{vmatrix} = \begin{vmatrix} k_r & 0 \\ 0 & k_z \end{vmatrix} = \begin{vmatrix} k_1 = k_2 & 0 \\ 0 & k_3 = k_4 \end{vmatrix}.$$

The terms $k_r$ and $k_z$ are called as principal thermal conductivity.

### *C. Governing Equations of Heat Flow*

With the thermal conductivity treated as a second-order tensor mentioned above, the system of nonhomogeneous HCE under a nonhomogeneous boundary condition in cylindrical coordinate system is written as

$$k_1 \frac{\partial}{r\partial r}\left(r\frac{\partial \mathbf{T}}{\partial r}\right) + k_3 \frac{\partial^2 \mathbf{T}}{\partial z^2} + \mathbf{G} = \frac{1}{\tilde{\alpha_d}} \frac{\partial \mathbf{T}}{\partial t} \tag{3}$$

in the region $a \le r \le b$, $0 \le z \le \ell$, $t > 0$. At the inner cylindrical surface ($r = a$, $t > 0$)

$$-k_1 \frac{\partial \mathbf{T}}{\partial r} + h_1 \mathbf{T} = \mathbf{f}_1(z,t). \tag{4}$$

At the outer cylindrical surface ($r = b$, $t > 0$)

$$k_2 \frac{\partial \mathbf{T}}{\partial r} + h_2 \mathbf{T} = \mathbf{f}_2(z,t). \tag{5}$$

At the bottom flat surface ($z = 0$, $t > 0$)

$$-k_3 \frac{\partial \mathbf{T}}{\partial z} + h_3 \mathbf{T} = \mathbf{f}_3(r,t). \tag{6}$$

At the top flat surface ($z = \ell$, $t > 0$)

$$k_4 \frac{\partial \mathbf{T}}{\partial z} + h_4 \mathbf{T} = \mathbf{f}_4(r,t). \tag{7}$$

In the region $a \le r \le b, 0 \le z \le \ell$, and $t = 0$

$$\mathbf{T} = \mathbf{F}(r, z). \tag{8}$$

Equations (3)–(8), represent the general BVP of HCE with convection at all four boundary surfaces.

In the above equations, temperature $\mathbf{T}$, is a function of space variables $r$ and $z$, and time variable $t$ (i.e., $\mathbf{T} \equiv \mathbf{T}(r, z, t)$). The term $\mathbf{G}$ is the heat source function, and has been modified here to take care of variation of resistivity of copper with temperature. The heat source term $G$ can be of the form

$$\begin{aligned} G &= \mathbf{g_0}(1 + \varrho_t(T - T_0)) \\ &= \mathbf{g_0} - \mathbf{g_0}\varrho_t T_0 + \mathbf{g_0}\varrho_t T = G_0 + \mathbf{g_0}\varrho_t T \end{aligned} \tag{9}$$

where $\varrho_t$ is the temperature coefficient of electrical resistance of copper wire in ${}^0C^{-1}$. With this representation, the function $G$ becomes temperature dependent, distributed, heat source. For the sake of mathematical convenience and to provide a reference for the heat source function, the constant $G_0$ is included to replace the constant part of (9).

The term $\mathbf{F}(r, z)$ represents the initial function for transient heat conduction problem. The term $\tilde{\alpha_d} = (1/\rho_{\rm eq} C p_{\rm eq}) = \alpha_d/\mathbf{K}$, where $\alpha_d$ is the diffusivity. The constant $\mathbf{K}$ shall be deduced in Section II-D, which can be identified with *equivalent thermal conductivity*.

The time-dependent boundary functions $\mathbf{f}_1 \ldots \mathbf{f}_4$, derived from Newton's law of cooling, are of the following form:

$$\mathbf{f}_i(z, t) \equiv \mathbf{f}_i^{(I)}(z) + \mathbf{f}_i^{(F\sim I)}(z)\left[1 - e^{-(t/\tau)}\right]. \tag{10}$$

The degenerate form in steady state, along the axial direction, is shown to be as in (11)

$$\mathbf{f}_i(z) = h_i \mathbf{T} z_i = h_i \times (T_{\rm b} + m_{si} z) \tag{11}$$

where $\mathbf{f}_i^{(I)}(z)$ is the initial temperature at time $(t = 0)$ and $\mathbf{f}_i^{(F\sim I)}(z)$ is the difference between final steady-state $(t = \infty)$ and initial steady-state $(t = 0)$ temperature. The term $T_b$ is the temperature at the bottom of the disc or layer, as applicable. Term $m_{si}$ is the axial temperature gradient. $\tau$ is the time constant (TC) of the thermal process.

Similarly, functions $\mathbf{f}_3(r)$ and $\mathbf{f}_4(r)$ representing temperature across bottom and top surfaces, in steady state, are of the form of $\mathbf{f}_j(r) = h_j \times (T_{\rm b}\ or\ T_{\rm top})$. Heat-transfer coefficients (**htc**) $h_1 \ldots h_4$, are different across all four surfaces, the values of which can be calculated by using heat-transfer empirical relations given in [1].

### D. Calculation of HST

*1) Method I:* Now introducing following independent variables:

$$r = \left(\frac{\mathbf{K}}{k_1}\right)^{(1/2)} r'; \quad z = \left(\frac{\mathbf{K}}{k_3}\right)^{(1/2)} z' \tag{12}$$

where $\mathbf{K}$ is a constant (called an equivalent thermal conductivity). Substituting (12) in (3), after rearrangement

$$\mathbf{K}\frac{\partial}{r'\partial r'}\left(r'\frac{\partial \mathbf{T}}{\partial r'}\right) + \mathbf{K}\frac{\partial^2 \mathbf{T}}{\partial z'^2} + \mathbf{G} = \frac{1}{\tilde{\alpha_d}}\frac{\partial \mathbf{T}}{\partial t} \tag{13}$$

where the constant $\mathbf{K}$ can be choosen as

$$\mathbf{K} = \sqrt{k_1 k_3}. \tag{14}$$

Here, the transformed variables $r'$ and $z'$ have been used to demonstrate the transformation. For notational simplicity, variables $(r, z)$ have been used in place of $(r', z')$ in the rest of the text and the HC (13) can be rewritten as

$$\frac{\partial}{r\partial r}\left(r\frac{\partial \mathbf{T}}{\partial r}\right) + \frac{\partial^2 \mathbf{T}}{\partial z^2} + \frac{\mathbf{G}}{\mathbf{K}} = \frac{1}{\alpha_d}\frac{\partial \mathbf{T}}{\partial t}. \tag{15}$$

The boundary conditions and initial condition still remain the same as (4)–(8). The HCE (15) is similar to the HCE proposed by the authors earlier [1].

*a) Steady-State Condition:* The HST in steady state can be computed from degenerated form of HC (15), which is as under

$$\frac{\partial}{r\partial r}\left(r\frac{\partial \mathbf{T}}{\partial r}\right) + \frac{\partial^2 \mathbf{T}}{\partial z^2} + \frac{\mathbf{G}}{\mathbf{K}} = 0; \quad a \le r \le b,\ 0 \le z \le \ell \tag{16}$$

where the time $t$ is absent. The applicable boundary conditions are the same as in (4)–(7) except that the time (variable) has been suppressed. These equations can be solved using finite Hankel and Fourier transforms w.r.t the $r$ and $z$ variables, respectively. Finite Hankel and Fourier transforms (FHT and FFT) of steady state (16) have been taken; the transformed equation is the form of

$$\begin{aligned} \overline{\overline{\mathbf{T}}}(\beta_n, \alpha_m) = {} & \frac{1}{\left(\alpha_m^2 + \beta_n^2 - \frac{\varrho_t \mathbf{g_0}}{\mathbf{K}}\right)} \\ & \times \left[\frac{\overline{\mathbf{f}}_1(\alpha_m)}{k_1}\{r\mathbf{K}_0(\beta_n, r)\}|_{r=a}\right. \\ & + \frac{\overline{\mathbf{f}}_2(\alpha_m)}{k_2}\{r\mathbf{K}_0(\beta_n, r)\}|_{r=b} \\ & + \frac{\overline{\mathbf{f}}_3(\beta_n)}{k_3}\{\mathbf{M}(\alpha_m, z)\}|_{z=0} \\ & \left. + \frac{\overline{\mathbf{f}}_4(\beta_n)}{k_4}\{\mathbf{M}(\alpha_m, z)\}|_{z=\ell} + \frac{\overline{\overline{\mathbf{G}}}_0}{\mathbf{K}}\right]. \end{aligned} \tag{17}$$

The inversion has been operated on (17). The steady-state temperature has been obtained, a double summation series

$$\mathbf{T}(r, z) = \sum_{n=1}^{\infty}\sum_{m=1}^{\infty} \overline{\overline{\mathbf{T}}}(\beta_n, \alpha_m)\mathbf{K}_0(\beta_n, r)\mathbf{M}(\alpha_m, z) \tag{18}$$

where $\mathbf{K}_0(\boldsymbol{\beta}_n, r)$ and $\mathbf{M}(\alpha_m, z)$ are kernel functions and have been used for finite Hankel and Fourier transform, respectively. In (17), $\overline{\mathbf{f}}_1$ and $\overline{\mathbf{f}}_2$ represent the finite Fourier transforms of $\mathbf{f}_1$ and $\mathbf{f}_2$. $\overline{\mathbf{f}}_3$ and $\overline{\mathbf{f}}_4$ are finite Hankel transforms of $\mathbf{f}_3$ and $\mathbf{f}_4$. The term $\overline{\overline{\mathbf{G}}}_0$ is the double transform of the constant part of source function $\mathbf{G}_0$, w.r.t. $\mathbf{K}_0(\boldsymbol{\beta}_n, r)$ and $\mathbf{M}(\alpha_m, z)$. To determine the

accuracy of estimation, transformation and inverse transformation of different types of functions (boundary, source, and initial function) w.r.t. kernel functions described are considered. Later, it has been checked as to what the number of terms should be to obtain a desired accuracy. Also, it can be shown that the terms of double summation form a highly converging series. The results on the convergence of the summation have been given in Appendix B.

The mathematical expression of the kernel functions described has been included in Appendix A. The parameters $\beta_n$ and $\alpha_m$, known as the eigenvalues are *positive* roots of transcendental (19) and (20), respectively

$$\frac{\beta_n k_1 J_1(\boldsymbol{\beta}_n a) + h_1 J_0(\boldsymbol{\beta}_n a)}{h_2 J_0(\boldsymbol{\beta}_n b) - k_2 \boldsymbol{\beta}_n J_1(\boldsymbol{\beta}_n b)} - \frac{\beta_n k_1 Y_1(\boldsymbol{\beta}_n a) + h_1 Y_0(\boldsymbol{\beta}_n a)}{h_2 Y_0(\boldsymbol{\beta}_n b) - k_2 \boldsymbol{\beta}_n Y_1(\boldsymbol{\beta}_n b)} = 0 \quad (19)$$

$$\tan(\alpha_m \ell) - \frac{\alpha_m \left(\frac{h_3}{k_3} + \frac{h_4}{k_4}\right)}{\alpha_m^2 - \frac{h_3}{k_3}\frac{h_4}{k_4}} = 0. \quad (20)$$

*b) Transient (Unsteady) State:* The conduction under unsteady state can also be described by the system of (15) and (4)–(8). Time-dependent boundary functions were assumed in the form of (10). To solve the unsteady equation, the temperature at $t = 0$, called initial function, can be calculated by solving the steady-state problem of initial state. In the present work, the initial function $F(r, z)$ has been assumed to be of the following form (21):

$$F(r, z) = \psi(r) \times \ln r \times \phi(z). \quad (21)$$

The solution procedure of the unsteady-state problem using FHT and FFT is exactly similar to the steady-state case. By applying the combined transform to general HCE (15), the transformed equations will be as shown below

$$\frac{d\overline{\overline{\mathbf{T}}}(\beta_n, \alpha_m, t)}{dt} + \alpha_d \left(\alpha_m^2 + \beta_n^2 - \eta\right) \overline{\overline{\mathbf{T}}} = \overline{\overline{\mathbf{Q}}}(\beta_n, \alpha_m, t) \quad (22)$$

and $\overline{\overline{\mathbf{T}}}(\beta_n, \alpha_m, t) = \overline{\overline{\mathbf{F}}}(\beta_n, \alpha_m)$ for $t = 0$ where

$$\overline{\overline{\mathbf{Q}}}(\beta_n, \alpha_m, t) = \left[\frac{\overline{\mathbf{f}}_1(\alpha_m, t)}{k_1}\{r\mathbf{K}_0(\beta_n, r)\}|_{r=a} + \frac{\overline{\mathbf{f}}_2(\alpha_m, t)}{k_2}\{r\mathbf{K}_0(\beta_n, r)\}|_{r=b} + \frac{\overline{\mathbf{f}}_3(\beta_n, t)}{k_3}\mathbf{M}(\alpha_m, z)|_{z=0} + \frac{\overline{\mathbf{f}}_4(\beta_n, t)}{k_4}\mathbf{M}(\boldsymbol{\alpha}_m, z)|_{z=l} + \frac{\overline{\overline{\mathbf{G_0}}}}{\mathbf{K}}\right]\alpha_d.$$

The above (22) is a Leibnitz equation and can be solved and equated to give

$$\overline{\overline{T}}(\beta_n, \alpha_m, t) = e^{-\alpha_d\left(\alpha_m^2 + \beta_n^2 - \eta\right)t} \times \left[\overline{\overline{\mathbf{F}}}(\beta_n, \alpha_m) + \int_0^t \overline{\overline{\mathbf{Q}}}(\beta_n, \alpha_m, t') e^{\alpha_d\left(\alpha_m^2 + \beta_n^2 \eta\right)t'} dt'\right]. \quad (23)$$

The temperature distribution $\mathbf{T}(r, z, t)$ is calculated as follows:

$$\mathbf{T}(r, z, t) = \sum_{n=1}^{\infty}\sum_{m=1}^{\infty} \mathbf{K}_0(\beta_n, r)\mathbf{M}(\alpha_m, z) e^{-\alpha_d\left(\alpha_m^2 + \beta_n^2 - \eta\right)t} \times \left[\overline{\overline{\mathbf{F}}}(\beta_n, \alpha_m) + \int_0^t \overline{\overline{\mathbf{Q}}}(\beta_n, \alpha_m, t') e^{\alpha_d\left(\alpha_m^2 + \beta_n^2 \eta\right)t'} dt'\right]. \quad (24)$$

where the term $\eta$ is equal to $\varrho_t \mathbf{g_0}/\mathbf{K}$.

*2) Method II:* The variable transformation defined by (12) distorts the boundary functions, thereby the circular region becomes an elliptic one [15]. The transformation of the space variable is approximately correct for a solid of smaller volume. However, the more rigorous, closed form solution of the GHC, (3), has been solved by using the FHT and FFT, where the kernel functions $\mathbf{K}_0(\beta_n, r)$, $\mathbf{M}(\alpha_m, z)$ and eigenfunctions (19), (20) remain the same.

*c) Steady-State Condition:* With generalized heat source function (9), the combined transformation of temperature in the steady-state case (17) is modified to (25)

$$\overline{\overline{\mathbf{T}}}(\beta_n, \alpha_m) = \frac{1}{(k_1\beta_n^2 + k_3\alpha_m^2 - \varrho_t \mathbf{g_0})} \times \Big[\overline{\mathbf{f}}_1(\alpha_m)\{r\mathbf{K}_0(\beta_n, r)\}|_{r=a} + \overline{\mathbf{f}}_2 + (\alpha_m)\{r\mathbf{K}_0(\beta_n, r)\}|_{r=b} + \overline{\mathbf{f}}_3(\beta_n)\{\mathbf{M}(\alpha_m, z)\}|_{z=0} + \overline{\mathbf{f}}_4(\beta_n)\{\mathbf{M}(\alpha_m, z)\}|_{z=\ell} + \overline{\overline{\mathbf{G}}}_0\Big]. \quad (25)$$

*d) Transient (Unsteady) State:* Similarly, the combined transformation of temperature in case of transient (23) is modified to (26)

$$\overline{\overline{\mathbf{T}}}(\beta_n, \alpha_m, t) = e^{-\tilde{\alpha_d}\left(k_1\beta_n^2 + k_3\alpha_m^2 - \varrho_t \mathbf{g_0}\right)t} \times \left[\overline{\overline{\mathbf{F}}}(\beta_n, \alpha_m) + \int_0^t \overline{\overline{\mathbf{Q}}}(\beta_n, \alpha_m, t') \times e^{\tilde{\alpha_d}\left(k_1\beta_n^2 + k_3\alpha_m^2 - \varrho_t \mathbf{g_0}\right)t'} dt'\right] \quad (26)$$

where

$$\overline{\overline{\mathbf{Q}}}(\beta_n, \alpha_m, t) = \Big[\overline{\mathbf{f}}_1(\alpha_m, t)\{r\mathbf{K}_0(\beta_n, r)\}|_{r=a} + \overline{\mathbf{f}}_2(\alpha_m, t)\{r\mathbf{K}_0(\beta_n, r)\}|_{r=b} + \overline{\mathbf{f}}_3(\beta_n, t)\mathbf{M}(\alpha_m, z)|_{z=0} + \overline{\mathbf{f}}_4(\beta_n, t)\mathbf{M}(\boldsymbol{\alpha}_m, z)|_{z=l} + \overline{\overline{\mathbf{G}}}_0\Big]\tilde{\alpha}_d.$$

The steady-state and unsteady-state temperature can be obtained by taking the combined inverse transform of (25) and (26), as defined in (18) and (24).

### *E. Calculation of Heat-Transfer Coefficients*

The calculation of **htc** in case of oil-natural (ON) mode has been discussed in some detail in [1]. The heat-transfer empirical formulation for calculation of **htc** in OF modes has also been given.

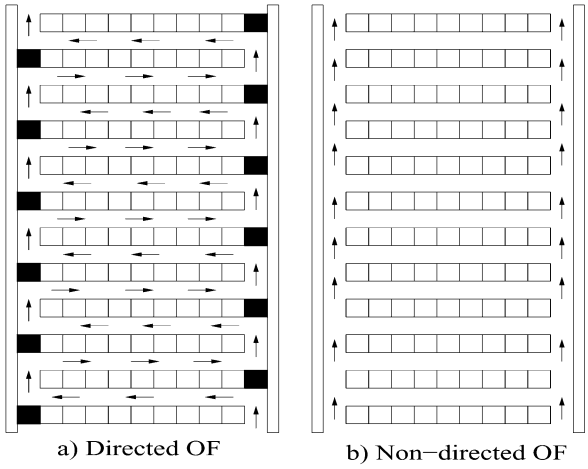


Fig. 3. Directed and nondirected OF modes in a disc winding.

The following assumptions have been made in the calculation of **htc** in the ducts provided in the disc-type windings (Fig. 3(a) and (b)) under forced-oil (OF) modes of heat transfer (DOF and NDOF).

- The cooling in OF mode is due to a mixed mode (natural and forced) convection.
- While the oil-flow velocity in both vertical and horizontal ducts has been assumed to be equal in the DOF mode and NDOF mode. The flow velocity in horizontal ducts is assumed negligible compared to velocity in the vertical ducts.
- In case of DOF mode, the **htc** was assumed to be a function of both heat flux through the surface and the oil-flow velocity. The mechanism of heat transfer in this mode of cooling is same in both axial and radial direction of the disc.
- In case of NDOF mode, the **htc** in the vertical duct (Fig. 3) has been estimated by the same formula as for DOF. But the convection of heat in the horizontal ducts has been assumed to be a purely natural type.

## III. Results and Discussions

### A. Steady-State Thermal Performance

The steady-state performance has been simulated by a software program using mathematical code. While on this point, the authors wish to point out that the results obtained in this work seem to be in reasonable qualitative agreement with some of the published experimental results viz. [9]. However, actual calculations for comparison could not be performed for paucity of design details in these papers. The applicability of the model has also been verified on transformers of the following ratings:

- 25/32 MVA (ONAN/ONAF);
- 22.5 MVA (ONAN).

The cu-loss in the winding per disc/layer of the above transformers has been tabulated in Table II. The total losses in transformer I at 32 MVA are 210 kW (0.82%). The total losses in transfomer II are 81 kW (about 0.45%). It can also be seen from this table that although the cu-loss in the 22.5-MVA transformer is very less compared to the other, the dimensions of high-voltage disc of two transformers are comparable.

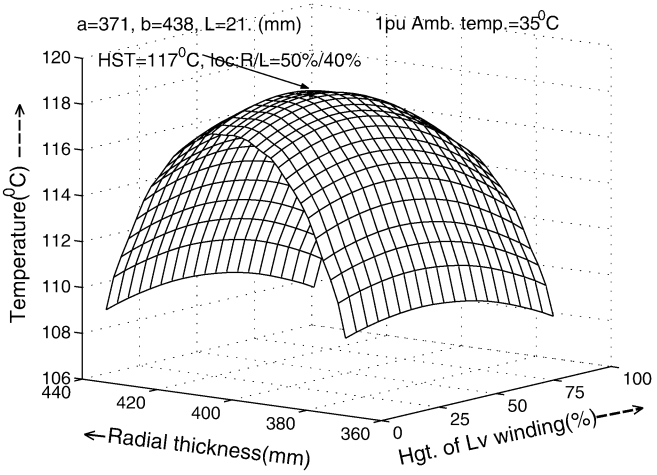


Fig. 4. Temperature distribution of a high-voltage disc.

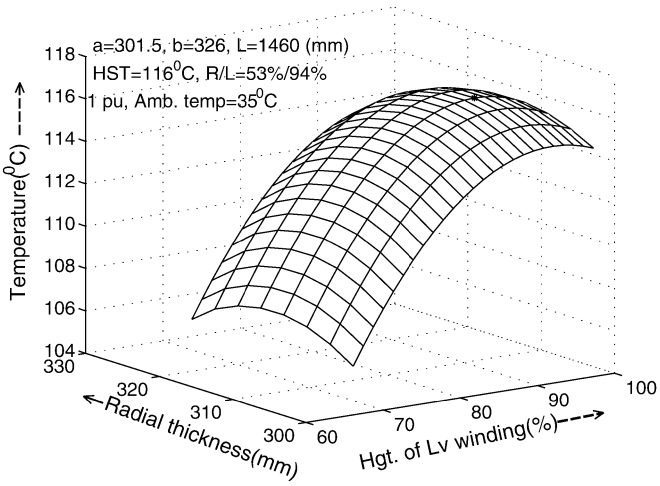


Fig. 5. Temperature distribution of low-volatge (LV) winding layer.

While on this aspect, the authors wish to point out that the IEEE loading guide and other similar documents offer empirical relations for the calculation of the HST based on per-unit load. The formulations tend to ignore the possibilities of two transformers which are rating-wise identical but have a different winding structure and varying heat loss/unit volume. The method suggested by the authors gives due representation for this omission and, hence, is believed to give more accurate estimates.

It may be observed that the maximum temperature occurs in the neighborhood of 35–45% of the axial and 50% of the radial thickness of the disc. Fig. 4 shows the spatial temperature distribution in a disc-type Hv winding. It may be observed that the HST would occur around the location of the second or the third disc from the top as surmised. But this position would change if there is oil stagnancy in the cooling ducts. In a layer winding, the HST occurs at around 85 to 95% of winding from the bottom. The spatial temperature distribution for a layer winding in $r$, $z$ plane has been shown in Fig. 5.

Under ONAN and ONAF modes of cooling, the magnitude and location of the HST at different loading have been shown in Tables III and IV. The computed value of the HST, arrived at

TABLE II
$I^2R$-LOSS CHARACTERISTICS OF TRANSFORMER WINDINGS AT 90°C

| transformer rating(MVA) | winding type | Cu-loss (Watt) | dimensions(mm) a, b, $\ell$ | remarks |
|---|---|---|---|---|
| 25/32 | Hv disc | 715 | 371, 438, 21 | per disc |
| 25/32 | Lv layer1 | 9500 | 263, 287.5, 1460 | per layer |
| 25/32 | Lv layer2 | 10700 | 301.5, 326, 1460 | per layer |
| 22.5 | Hv disc | 150 | 388, 473, 15.5 | per disc |
| 22.5 | Lv disc | 110 | 289, 359, 12 | per disc |

TABLE III
HST MAGNITUDE AND LOCATION IN ONAN

| 22.5 MVA transformer, Amb. temp.=35$^0$C, ON | | | | | | |
|---|---|---|---|---|---|---|
| pu load | detail description(M2) winding type | HST local | loc. $\mathcal{R}/\mathcal{L}$ | HST cal. (M2) | HST IEC | HST cal. (M1) |
| 1.0 | hvD | 91 | 45/49 | 94 | 113 | 92 |
| | lvD | 94 | 42/45 | | | |
| 1.25 | hvD | 116 | 45/49 | 120 | 140 | 115 |
| | lvD | 120 | 42/45 | | | |
| 1.5 | hvD | 142 | 50/45 | 147 | 172 | 142 |
| | lvD | 147 | 50/42 | | | |
| 1.8 | hvD | 182 | 50/43 | 185 | 215 | 178 |
| | lvD | 185 | 50/42 | | | |
| 2‡ | hvD | 205 | 50/39 | 214 | 245 | 202 |
| | lvD | 214 | 50/42 | | | |
| 2.2‡ | hvD | - | 50/39 | 244 | 280 | 230 |
| | lvD | 244 | 54/42 | | | |

‡:There are instances [16] in which large power transformer are loaded to as high as 2.5 pu although the limit there-on is 1.5 pu as per the IEEE guide.

TABLE IV
HST MAGNITUDE AND LOCATION IN ONAF MODE

| 25/32 MVA transformer, Amb. temp.=35$^0$C, ONAF | | | | | | |
|---|---|---|---|---|---|---|
| pu load | detail description(M2) winding type | HST local | loc. $\mathcal{R}/\mathcal{L}$ | HST cal. (M2) | HST IEC | HST cal. (M1) |
| | hvD | 117 | 52/40 | | | |
| 1.0 | lv1L | 122 | 45/94 | 122 | 114 | 127 |
| | lv2L | 115 | 53/94 | | | |
| | hvD | 138 | 52/40 | | | |
| 1.1 | lv1L | 134 | 45/93 | 138 | 127 | 144 |
| | lv2L | 132 | 45/93 | | | |
| | hvD | 153 | 52/40 | | | |
| 1.2 | lv1L | 156 | 45/93 | 156 | 142 | 162 |
| | lv2L | 153 | 52/93 | | | |
| | hvD | 176 | 52/38 | | | |
| 1.3 | lv1L | 199 | 49/91 | 199 | 191 | 193 |
| | lv2L | 195 | 49/91 | | | |
| | hvD | 209 | 52/38 | | | |
| 1.4 | lv1L | 230 | 49/91 | 230 | 228 | 228 |
| | lv2L | 228 | 49/91 | | | |
| | hvD | 71 | 54/38 | | | |
| 0.6 | lv1L | 69 | 43/95 | 71 | 72 | 72 |
| | lv2L | 69 | 53/95 | | | |
| | hvD | 95 | 51/38 | | | |
| 0.8 | lv1L | 93 | 44/94 | 95 | 92 | 101 |
| | lv2L | 94 | 50/94 | | | |

using the two methods described in Section II, has been compared. The results obtained using Method I have been indicated as (M1) and and Method II as (M2). Furthermore, a comparison has been made of the magnitude of HST computed from method I and II with HST computed using IEEE and IEC loading guide equations.

TABLE V
HST IN OIL-FORCED COOLING MODES

| 32 MVA transformer, Amb. temp.=35$^0$C, hvD, (M2) | | | | |
|---|---|---|---|---|
| pu load | cooling levels/types mode | $V_{oil}$ m/sec. | HST mag(local) | HST($\mathcal{R}/\mathcal{L}$) location |
| 1.5 | OD | 0.01 | 169 | 50/50 |
| | | 0.02 | 155 | 50/50 |
| | ND | 0.01 | 198 | 50/38 |
| | | 0.02 | 184 | 50/38 |
| 1.8 | OD | 0.01 | 222 | 50/50 |
| | | 0.02 | 203 | 50/50 |
| | ND | .01 | 253 | 51/38 |
| | | 0.02 | 237 | 50/38 |
| 2 | OD | 0.01 | 265 | 50/50 |
| | | 0.02 | 242 | 50/50 |
| | ND | 0.01 | 294 | 51/38 |
| | | 0.02 | 275 | 50/38 |
| 2.2 | OD | 0.01 | 314 | 50/50 |
| | | 0.02 | 287 | 50/50 |
| | ND | 0.01 | 338 | 51/38 |
| | | 0.02 | 318 | 50/38 |

TABLE VI
ESTIMATED TIME CONSTANT ($\tau$) OF TRANSFORMER WINDINGS

| Wdg. type | $\mathbf{g}_0$ $\frac{kW}{m^3}$ | $\rho_{eq}$ $\frac{kg}{m^3}$ | $\mathrm{Cp}_{eq}$ $\frac{J}{kg^oC}$ | $\beta_1$ | $\alpha_1$ | $\tau$ min. |
|---|---|---|---|---|---|---|
| hvD | 288 | 5640 | 482 | 45.9 | 33.4 | 5.01 |
| lv1L | 154 | 8000 | 410 | 41.9 | 2.03 | 4.15 |
| lv2L | 152 | 8050 | 410 | 39.7 | 2.03 | 5.13 |
| hvD | 66 | 7688 | 413 | 26.7 | 87.5 | 4.8 |
| lvD | 101 | 8000 | 410 | 27 | 90 | 4 |

More complex cooling modes involving DOFAF or NDOFAF (Table V) are also considered as they have practical significance. The estimated temperature of the hot spot and its location seem to be in line with the field measurements. However, there appears to be no published literature giving this information against which comparisons can be made.

### B. Unsteady-State Thermal Performance

From a practice standpoint, the thermal performance in dynamic loading and dynamic ambient are of great interest. It has been assumed here that the boundary surface temperature as well as oil temperature gradient depend on time as described by (24). Also, the method of calculation of the thermal parameters are exactly same to that in the steady-state case. In this case (transient case), the heating process in a transformer winding has been simulated by introducing a transient thermal load.

*1) Initial Function:* The initial function for transient heat-flow problem can be determined from the temperature distribution obtained from the steady-state solution. A typical polynomial of $r$ and $z$ has been found to effect this to a reasonable degree of accuracy as under

$$F(r,z) = 294.27z - 18\,908.13z^2 + 4673.26z^3 + 290.532\ln r - 4705.28r^2\ln r + 13\,064.2r^4\ln r + 37.66r^2z\ln r - 2733.99r^2z^2\ln r + 31\,830.25r^2z^3\ln r. \quad (27)$$

*2) Estimation of Winding Time Constant:* Equation (18) gives the temperature as a double summation, as indicated. In Appendix B, it has been shown that the terms of the summation converge quite rapidly. It is also seen that the first term of the summation is the dominant term (Tables VII and VIII).

TABLE VII
HST CALCULATED WITH DIFFERENT NO. OF TERMS OF THE SUMMATION

| hvD, a, b, $\ell$=371, 438, 21 mm | | | | | | | | |
|---|---|---|---|---|---|---|---|---|
| n | m | no. terms n×m | HST(M2) $^0$C | cordinate r | z | Fist few terms 1 | 2 | 3 |
| 10 | 10 | 100 | 119.096 | 403 | 9 | 144.2 | -3.2 | -3 |
| 20 | 20 | 400 | 118.272 | 403 | 9 | 144.2 | -3.2 | -3 |
| 30 | 30 | 900 | 118.396 | 403 | 9 | 144.2 | -3.2 | -3 |
| 30 | 30 | 900 | 118.396 | 403 | 9 | 144.2 | -3.2 | -3 |
| 40 | 40 | 1600 | 118.281 | 403 | 9 | 144.2 | -3.2 | -3 |
| 50 | 50 | 2500 | 118.364 | 403 | 9 | 144.2 | -3.2 | -3 |
| 150 | 70 | 10500 | 118.276 | 403 | 9 | 144.2 | -3.2 | -3 |
| 200 | 70 | 14000 | 118.271 | 403 | 9 | 144.2 | -3.2 | -3 |

TABLE VIII
HST CALCULATED WITH DIFFERENT NO. OF TERMS OF THE SUMMATION

| lvL, a, b, $\ell$=,263 287.5, 1460 mm, calculated at point(r,z)=(279,1320) | | | | | | | | |
|---|---|---|---|---|---|---|---|---|
| n | m | no. terms n×m | HST(M2) $^0$C | Fist few terms 1 | 2 | 3 | 5 | 7 |
| 10 | 10 | 100 | 133.169 | 48 | 6.3 | 40 | 25 | 10 |
| 20 | 20 | 400 | 117.699 | 48 | 6.3 | 40 | 25 | 10 |
| 30 | 30 | 900 | 125.282 | 48 | 6.3 | 40 | 25 | 10 |
| 40 | 40 | 1600 | 121.169 | 48 | 6.3 | 40 | 25 | 10 |
| 50 | 50 | 2500 | 123.813 | 48 | 6.3 | 40 | 25 | 10 |
| 60 | 60 | 3600 | 121.898 | 48 | 6.3 | 40 | 25 | 10 |
| 80 | 80 | 6400 | 122.190 | 48 | 6.3 | 40 | 25 | 10 |
| 100 | 100 | 10000 | 122.300 | 48 | 6.3 | 40 | 25 | 10 |
| 200 | 200 | 40000 | 122.659 | 48 | 6.3 | 40 | 25 | 10 |
| 300 | 300 | 90000 | 122.745 | 48 | 6.3 | 40 | 25 | 10 |

Therefore, the time constant of the transformer winding can be determined only from the first term of the summation.

$$\tau \approx \frac{1}{\rho_{\mathrm{eq}} C_p \mathrm{eq}\,(k_1\beta_1^2 + k_3\alpha_1^2 - \varrho_t \mathbf{g_0})}. \tag{28}$$

Referring to Table VI, the thermal time constant of winding is around 4.5–5 min. These values have been expressly calculated (and not assumed as was done earlier) using the thermal parameters of the winding.

## IV. CONCLUSION

1) Earlier, the authors proposed a heat conduction model for the estimation of HST. This paper presents a generalized version of the heat conduction (GHC) model. The BVP encountered here has been solved analytically using finite integral transform methods.
2) The rigorous theoretical approach for evaluating HST followed in this paper seems to correspond reasonably well with results of actual tests and onsite measurements [9]. As has already been pointed out, the comparison is only qualitative in nature, the quantitative comparison can be made only when the design data of the windings are available.
3) The heat source function has been taken as temperature dependent and has been directly incorporated in the HCE.
4) The thermal model presented here can predict the hot-spot location, with a higher degree of accuracy than was hither to possible. In a newly commissioned transformer, the prediction accuracy is even better.

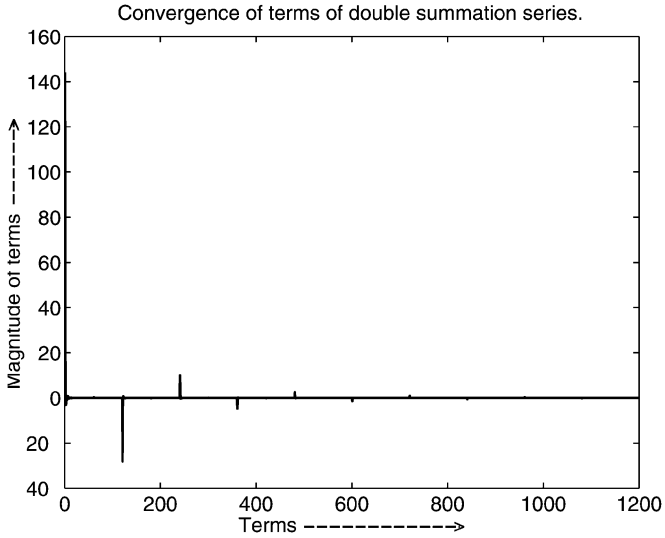


Fig. 6. Convergence of the summation (18).

5) The result of the study on the rate of convergence of double summation series indicates that the convergence is indeed quite rapid and nearly monotonic. Also, suggestions have been made as to the optimum numbers of terms to be considered to obtain sufficient accuracy.

## APPENDIX A
## KERNEL FUNCTIONS FOR FHT AND FFT

The kernel function $\mathbf{K}_0(\boldsymbol{\beta}_n, r)$, also known as normalized eigenfunction for $r$ variable, is the ratio of eigenfunction $\mathbf{R}_0(\boldsymbol{\beta}_n, r)$ to the square root of orthonormal $\mathbf{N}$. Mathematically

$$\begin{aligned}
\mathbf{K}_0(\boldsymbol{\beta}_n r) &= \frac{\mathbf{R}_0(\boldsymbol{\beta}_n r)}{\sqrt{\mathbf{N}}} \\
\mathbf{R}_0(\boldsymbol{\beta}_n r) &= \frac{J_o(\boldsymbol{\beta}_n r)}{h_2 J_0(\boldsymbol{\beta}_n b) - k_2 \boldsymbol{\beta}_n J_1(\boldsymbol{\beta}_n b)} \\
&\quad - \frac{Y_0(\boldsymbol{\beta}_n r)}{h_2 Y_0(\boldsymbol{\beta}_n b) - k_2 \boldsymbol{\beta}_n Y_1(\boldsymbol{\beta}_n b)} \\
\mathbf{N} &= \frac{b^2}{2}\left[\frac{h_2^2}{\boldsymbol{\beta}_n^2 k_2^2} + 1\right] R_0^2(\beta_n, b) \\
&\quad - \frac{a^2}{2}\left[\frac{h_1^2}{\boldsymbol{\beta}_n^2 k_1^2} + 1\right] R_0^2(\beta_n, a).
\end{aligned} \tag{29}$$

And the corresponding quantities for $z$ variable are as follows:

$$\begin{aligned}
\mathbf{M}(\boldsymbol{\alpha}_m, z) &= \frac{\mathbf{Z}(\boldsymbol{\alpha}_m, z)}{\sqrt{\mathbf{N}'}} = \frac{\cos\alpha_m z + \frac{h_3 \sin\alpha_m z}{k_3 \alpha_m}}{\sqrt{\mathbf{N}'}} \\
\mathbf{N}' &= \frac{1}{2}\left[\left(\frac{\alpha_m^2 + \frac{h_3^2}{k_3^2}}{\alpha_m^2}\right)\left(l + \frac{\frac{h_4}{k_4}}{\alpha_m^2 + \frac{h_4^2}{k_4^2}}\right) + \frac{\frac{h_3}{k_3}}{\alpha_m^2}\right].
\end{aligned} \tag{30}$$

The parameter $\beta_n$ and $\alpha_m$ are the *positive* roots of transcendental (19) and (20), respectively, which are known as eigenvalues.

## APPENDIX B
## ON THE CONVERGENCE OF SOLUTION

The rapidity of convergence of the solution has been considered in some detail. The results thereof are tabulated in Tables VII and VIII and have been shown diagrammatically in Fig. 6.

## REFERENCES


[1] M. K. Pradhan and T. S. Ramu, "Prediction of hottest spot temperature (HST) in power and station transformers," *IEEE Trans. Power Delivery*, vol. 18, pp. 1275–1283, Oct. 2003.

[2] R. Hurter and F. Viale, "Thermal aspects of large transformers, test procedures hot spot identification, permissible limits, their assessment in factory tests and service, overload limitations, effect of cooling system:-Presented in the name of study committee-12," in *Proc. CIGRE.12–13 30th Session*, vol. 1, 1984.

[3] J. Aubin, "Thermal aspects of transformers:-Presented in the name of study committee 12," in *Proc. CIGRE Paper, 12-1073 1990*, vol. 1, Aug./Sept. 1990.

[4] "Loading Guide for Mineral Oil-Immersed Power Transformer,", IEC-354, 1991.

[5] M. V. Thaden, S. P. Meheta, S. C. Tuli, and R. L. Grubb, "Temperature rise test on a OFAF core-form transformer, including loading beyond name plate," *IEEE Trans. Power Delivery*, vol. 10, pp. 913–919, Apr. 1995.

[6] W. Lampe, L. Pettersson, C. Ovren, and B. Wahlstrom, "Hot spot measurement in power transformers," in *Proc. CIGRE Paper, 12—02 30th Session*, vol. 1, 1984.

[7] W. J. Mcnutt, J. C. McIver, R. V. Snow, and D. J. Fallon, "Transformer loading capability information derived from winding hot spot measurements," in *Proc. Int. Conf. Large High Voltage Electrical System, 30th Session*, vol. 1, CIGRE, Paris, France, 1984, Paper, 12-08.

[8] "IEEE Loading Guide for Mineral Oil Immersed Transformer,", C57.91.1995, 1996.

[9] L. W. Pierce, "An investigation of the thermal performance of an oil filled transformer winding," *IEEE Trans. Power Delivery*, vol. 7, pp. 1347–1358, July 1992.

[10] ——, "Predicting liquid filled transformer loading capability," *IEEE Trans. Ind. Applicat.*, vol. 30, pp. 170–178, Jan./Feb. 1994.

[11] "IEEE Loading Guide for Mineral Oil Immersed Transformer, C57.91/Corrigenda,", Draft Corrigenda to C57.91-1995, 2001.

[12] *IEEE Guide for Determination of Maximum Winding Temperature Rise in Liquid-Filled Transformers*, IEEE Std. 1538-2000, Aug. 2000.

[13] G. Swift, T. S. Molinski, and W. Lehn, "A fundamental approach to transformer thermal modeling. Part-I: Theory and equivalent circuit," *IEEE Trans. Power Delivery*, vol. 16, pp. 171–175, Apr. 2001.

[14] S. A. Ryder, "A simple method for calculating winding temperature gradient in power transformers," *IEEE Trans. Power Delivery*, vol. 17, pp. 977–982, Oct. 2002.

[15] M. N. Ozisik, *Boundary Value Problem of Heat conduction*. Scranton, PA: International Textbook, 1968, pp. 467–475.

[16] H. Nordman and M. Lahtinen, "Thermal overload tests on a 400-MVA power transformer with a special 2.5-p.u. short time loading capability," *IEEE Trans. Power Delivery*, vol. 18, pp. 107–112, Jan. 2003.



**M. K. Pradhan** was born in Balasore, Orissa, India. He received the B.E. degree in electrical engineering from the University College of Engineering (UCE) Burla, Orissa, India, in 2000 and the M.Sc. degree in engineering from the High Voltage Engineering Department, Indian Institute of Science, Bangalore, India, in 2002.

His research interests include diagnostic testing and condition monitoring of power equipment, and application of artificial intelligence to condition monitoring of power equipment.

**T. S. Ramu** was born in Bangalore, India. He received the B.E., M.E., and Ph.D. degrees from Mysore University, Bangalore, India, Indian Institute of Science (I.I.Sc.), Bangalore, India, and the Indian Institute of Technology (IIT), Madras, India.

Currently, he is a Professor with the Department of High Voltage Engineering at the I.I.Sc.